SCIENTIFIC REPORTS

OPEN

SUBJECT AREAS:
MAGNETIC DEVICES
ELECTRONIC DEVICES
ELECTRONIC PROPERTIES AND DEVICES

Received
7 August 2014

Accepted
25 November 2014

Published
23 December 2014

Correspondence and requests for materials should be addressed to Z.Zg. (lgzzhang@sohu.com)

Magnetic structure and Magnetic transport Properties of Graphene Nanoribbons With Sawtooth Zigzag Edges

D. Wang[1], Z. Zhang[1], Z. Zhu[1] & B. Liang[1,2]

[1]Institute of Nanomaterial & Nanostructure, Changsha University of Science and Technology, Changsha 410114, China, [2]School of Automotive & Mechanical Engineering, Changsha University of Science and Technology, Changsha 410114, China.

The magnetic structure and magnetic transport properties of hydrogen-passivated sawtooth zigzag-edge graphene nanoribbons (STGNRs) are investigated theoretically. It is found that all-sized ground-state STGNRs are ferromagnetic and always feature magnetic semiconductor properties, whose spin splitting energy gap E_g changes periodically with the width of STGNRs. More importantly, for the STGNR based device, the dual spin-filtering effect with the perfect (100%) spin polarization and high-performance dual spin diode effect with a rectification ratio about 10^{10} can be predicted. Particularly, a highly effective spin-valve device is likely to be realized, which displays a giant magnetoresistace (MR) approaching 10^{10}%, which is three orders magnitude higher than the value predicted based on the zigzag graphene nanoribbons and six orders magnitude higher than previously reported experimental values for the MgO tunnel junction. Our findings suggest that STGNRs might hold a significant promise for developing spintronic devices.

Spintronic devices (STDs), using spin instead of charge as an information carrier, have recently attracted tremendous attention within the scientific community. Due to unique electronics as well as magneto-electronics properties, such as a weak spin-orbital coupling and long spin correlation length for electrons, which are some key features for developing STDs[1–3], the two-dimensional planar graphene and the corresponding quasi-unidimensional graphene nanoribbons (GNRs) have been extensively studied[1–7]. Especially for zigzag graphene nanoribbons (ZGNRs), one predicts that they will play an important role in spintronic applications. Ground-state ZGNRs exhibit ferromagnetically (FM) ordered states at each edge individually due to the unsaturated π electron existing for each edge carbon atom but antiferromagnetic (AFM) coupling between opposite edges, leading to a spin-polarized semiconducting behavior with zero net spin[4], thus their applications in STDs are severely limited. Heretofore, many effective approaches, such as edge modifications[8], doping[9], introducing topologic defects[10], and applying an external electrical field[4] or magnetic field[5], have been proposed to break the spin degeneracy and stabilize ferromagnetic (FM) state in ZGNRs, achieving metallic or half- metallic features accordingly. Based on these ways, some important phenomena are found and promising STDs, such as giant magnetoresistance devices and conductance switchers[5], spin-filtering devices[6], bipolar spin diodes[6,7], spin-polarized current amplifiers[7], and bipolar field-effect spin-filtering devices[11], are designed theoretically.

However, in fact, the realistic applications of the ZGNR magnetism and the above methods to obtain a favorable magnetic ordering might not be feasible. Generally, a very large electrical field is required to split the spin-degenerated band structures and achieve a half-metallicity experimentally. The theoretical predicted magnetic moment for edge carbon atoms is not very strong[12], so that the spin-polarized states of the ZGNRs become unstable to be transformed to the spin-unpolarized state in the presence of ballistic current through the ZGNRs[13,14] or at finite temperatures[15]. It was estimated that the magnetic states can only be stabilized at temperatures $T < 10K$[16,17], and become paramagnetic(PM) behaviors as T increases, which has been confirmed experimentally[18]. And also, as reported in previous works[5–7], STD effects based on ZGNRs essentially occur for geometrically symmetrical ZGNRs with respect to the axis due to the intrinsic transmission selection rule of the wave function of spin subbands near the Fermi level, but not for geometrically asymmetrical ZGNRs. Particularly, realizing the specific magnetic device features needs the externally magnetic field simultaneously applied on left and right ZGNR electrodes to create the [1,-1] magnetic configurations[5–7], however, it is difficult to limit two

magnetic fields with the opposite direction in two local nano-scale regions, which might exceed those available experimentally[19]. Additionally, heteroatom doping would influence the mobility and spin correlation length of carriers, even resulting in a spin flip, and edge modification might weaken the geometrical structure stability. Therefore, designing graphene-based systems to have a large ground-state magnetic moment and become experimentally feasible STDs remains a challenge.

In this paper, we present investigations on magnetic structure and magnetic transport properties for the graphene nanoribbons (GNRs) with sawtooth (ST) zigzag edges (STGNRs)[20] and passivated by mono-hydrogen atom[21], which is related to modified-edge GNRs[22,23]. It is found that at a FM ground state they are all a magnetic semiconductor. In particular, unique band overlap pattern for two electrodes and its particular sensitivity to a switching magnetic field lead to the dual spin-filtering effect with the perfect (100%) spin polarization and high-performance dual spin diode effect with a rectification ratio about 10^{10}, as well as a highly effective spin-valve device feature with a giant magnetoresistace (GMR) value approaching 10^{10}% can be observed.

Results

Fig. 1 illustrates the schematic structure of STGNRs (m, n), and the rectangle box drawn with a dotted line denotes a unit cell. STGNRs can be view as the armchair graphene nanoribbons (AGNRs) being tailored or introducing defects at their edge to form zigzag edges with a large sawtooth periodically. Current nano-size lithographic techniques have provided the possibility for cutting or patterning graphene into well-defined geometric structures with atom precision, for example, the controlled formation of sharp zigzag edges in GNRs has been recently fabricated experimentally[24]. The dangling bond on each edge carbon atom for STGNRs (m, n) is all saturated by single hydrogen (H) atom in order to retain the sp^2 hybridization of carbon atoms. Here, two integers, m and n, are used to represent the unit-cell size of STGNRs, which are the number of hexagonal rings along the m and n directions, respectively, as shown in Fig. 1, corresponding to the width of nanoribbon and the length of a large sawtooth at edge. It is important to note that to form a periodic nanoribbon structure, n must be an odd number and equal to or bigger than 3, i.e., $n \geq 3$, and both m and n satisfy $m - n \geq 1$ to assure STGNRs being the same width for the whole nanoribbon. Further, we construct device models by the STGNRs to investigate magnetic transport behaviors, where a device is divided into three regions: left electrode, right electrode, and the scattering region (the device region). Each electrode is represented by a unit cell of STGNR along the axis and descried by self-energies, and the scattering region is involved in the self-consistent cycle for calculations and takes into account the interface coupling and screening layer effects.

We firstly investigate electronic and magnetic structures of STGNRs with STGNR(5,3) as example. The isosurface plots for the spin polarized density ($\nabla\rho = \rho_\alpha - \rho_\beta$) of the FM and AFM states are shown in Fig. 2(a) and (b), respectively, where ρ_α and ρ_β denote the electron density of majority spin (α) (red) and minority spin (β) (blue), respectively. For the FM state as shown in Fig. 2(a), all the carbon atoms display spin-polarized states, specially, there exists a spin parallel coupling between both edges. While for the AFM state, as shown in Fig. 2(b), STGNR displays FM ordering at each edge carbon atoms individually, but AFM coupling between both edges, similarly to ground-state ZGNRs. Our calculations show that the FM state is a ground state, its total energy is found to be 31 meV per unit cell lower than the AFM state. These results are easy to be understood. For graphene, the spin of the A and B sublattices is antiparallel. In a STGNR, the edge carbon atoms always belong to the same sublattice, A sublattice, except for carbon atoms with the armchair bond at corners. The polarization of carbon atoms in the A sublattice, especially at the edges, is much stronger than that in the B sublattice, which is actually due to the unsaturated bond of those atoms, even after they are hydrogenated. Upon the strong interactions between the carbon atoms, the inside atoms are also spin-polarized. For a STGNR (m, n), the number of A-type carbon atoms and B-type carbon atoms is of unbalanced, they are $N_A = \frac{n+1}{2}(2m-n+2) + (n-1)$ and $N_B = \frac{n+1}{2}(2m-n+2)$ per unit cell, respectively. Thus the difference of the number for two types of carbon atoms is N_A-N_B = n-1, independent of m. According to Lieb's theorem, total net spin magnetization of a graphene structure is $M = \frac{1}{2}|N_A - N_B|g\mu_B$, where $g \approx 2$ for the electron, μ_B is the Bohr magneton. Applying this rule, we can obtain that the magnetic moment is $2\mu_B$ for STGNR(5, 3). Our calculations on Mulliken Population involving the spin polarization show that the magnetic moment for STGNR(5, 3) is about $1.85\mu_B$ per unit cell, which basically agrees with Lieb's theorem. This slight smaller value is because the interactions between edge carbon atoms and H atoms induce a rearrangement of electron spins of carbon atoms[25].

The spin-resolved band structure (BS), the density of states (DOS), and the projected density of states (PDOS) for STGNR(5, 3) at the FM ground state are exhibited in Fig. 2 (c). The middle and right panels display the atom-PDOS and orbital-PDOS, respectively. As can be seen, α- and β-spin subbands are prominently split, but no subband (or DOS) crosses (or touches) the Fermi level, and the conduction and valance bands nearest to the Fermi level belong to

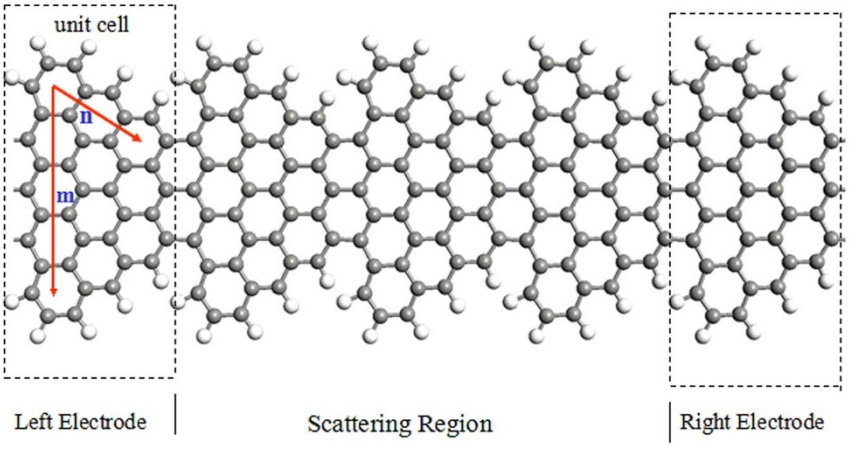

Figure 1 | The schematic diagram of geometrical structures and the constructed device model for STGNRs(m, n), the dashed box indicates the unit cell, and (m, n) denotes the size of a unit cell.

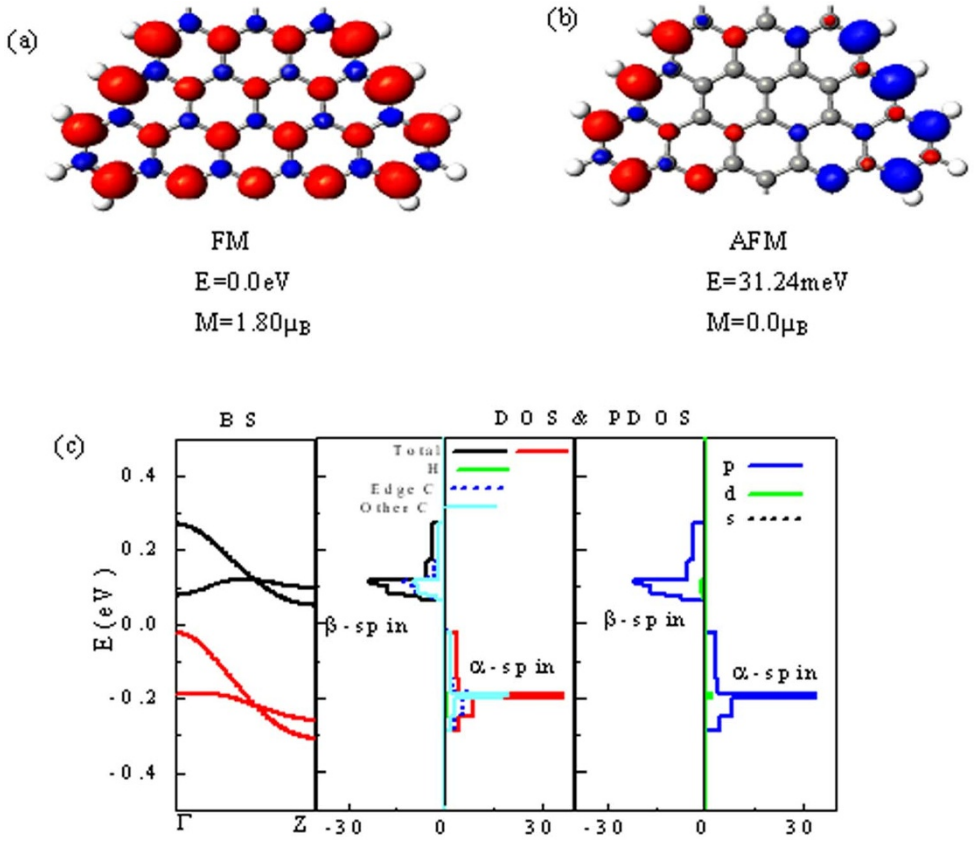

Figure 2 | Electronic and magnetic structures of STGNR(5,3). Isosurface plots of the spin density ($\nabla\rho = \rho_\alpha - \rho_\beta$) of the FM ground state (a) and AFM state (b) for an optimized H-STGNR(5,3). Values for red (α-spin) and blue (β-spin) isosurfaces are $\pm 0.01|e|/Å^3$, respectively. (c) The band structure (BS), density of states (DOS), and projected density of states (PDOS) for STGNR(5,3). PDOS includes the atom-PDOS and orbital- PDOS.

β- and α-spin states, respectively. This indicates that STGNR(5, 3) features the properties of bipolar magnetic semiconductors (BMS)[11] with a well-defined spin splitting energy gap E_g, ~75 meV. The BMS is an important material for realizing bipolar spin-filtering (BSF) devices[11]. The middle and right panels for the PDOS suggest that the DOS around the Fermi level is mainly derived from p (π) orbital (the s- and d-orbital PDOS is negligible small) of C atoms(at both edges and others).

To find the size effects, the band structure and spin splitting energy gap as a function of geometrical parameters, m and n, corresponding to the width of nanoribbon and the length of a large sawtooth at edge for STGNRs, are shown in Fig. 3(a–c). It is clear that the magnetic semiconducting behaviors for all STGNRs are always preserved regardless of the value of m and n. Interestingly, the spin splitting energy gap E_g changes periodically with the value of m by 3 as a period, and satisfies $E_g^{3i+1} > E_g^{3i} > E_g^{3i-1}$ (i is a positive integer), similarly to the case of AGNRs for the gap alteration with width. With increasing the value of n, the spin splitting energy gap E_g drops at n=5 then rises sharply.

For realistic applications of magnetic materials, the magnetic stability is an important aspect that needs to be considered. As we know, the paramagnetic response of a system is described by the Pauli susceptibility which depends only on the electronic density of states at the Fermi level (Stoner instability)[26]. STGNRs have almost zero DOS at the Fermi level at the FM ground-state as shown in Figs. 2 (c), thus giving rise to a higher ground-state magnetic stability for STGNRs than that for the FM state of ZGNRs with finite DOS at the Fermi level[5]. To further investigate a thermal stability, the energy difference ΔE_{mag} between the AFM and FM states as a function of m and n is drawn in Fig. 3(d). As mentioned above, the FM is the ground state (GS) with a lowest energy, while the AFM is the second-lowest energy state (GS+1), and the nonmagnetic state possesses a highest energy (GS+2)(not exhibited here). Generally, the thermal stability of materials is regarded to be related to ΔE_{mag}. As can be seen, ΔE_{mag} decreases with increasing m, but arises monotonically with increasing n, this is easy to be understood. When the value of m increases to form a wider ribbon, the edge magnetic coupling (exchange interaction) is weakened accordingly to display pristine AGNR properties partially. Conversely, increasing n means increasing the length of zigzag edges and in turn decreasing their spacing, so that the two-edge magnetic coupling is strengthen unambiguously. The thermal stability is usually quantified by the Curie temperature T_c based on the mean-field theory and Heisenberg model[27], $T_c = 2\Delta/3k_B$, whereΔ is the energy required to flip one spin to the GS+1 state. We can obtain Δ = 12.24 meV for STGNR (4, 3), leading to $T_c \sim 95$ K. It is almost 10 times as large as ZGNRs by the experiment value $T_c < 10K$[16,17], but still much below room temperature.

To develop future STDs based on STGNRs, it is highly desirable to fully understand their intrinsic magnetic transport properties under bias. The constructed device model is shown in Fig. 1, as stated above. Here, two types of magnetic configurations are considered, respectively : (1) P configuration, namely, whole device is taken as a FM ground state, and the spin ordering for two electrodes in parallel points to the same direction. α- and β-spin states are major and minor spin components, respectively. (2) AP configuration, i.e., an externally switching magnetic field is applied perpendicular to the plane of the right electrode to switch its spin ordering antiparallel to the left electrode, namely, the left electrode is still α-spin polarized but the right one is turned to be β-spin polarized, in order to demonstrate the response of STGNRs to an application of the magnetic field. Furthermore, the spins across the magnetic domain wall in the scattering region is set in a collinear case for calculations. We still

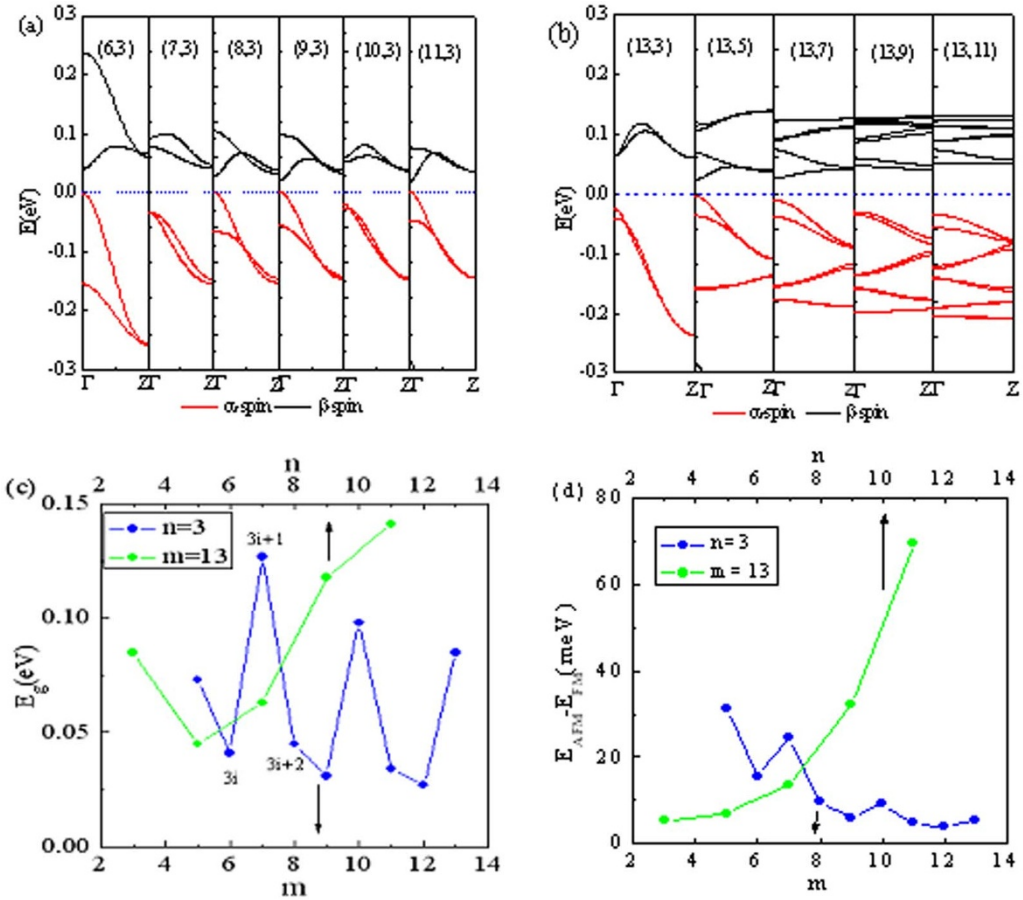

Figure 3 | Size effects for STGNRs(m,n). (a), (b), (c), and (d) show the change of the band structures, spin splitting energy gap, and energy difference ΔE_{mag} between the AFM state and the FM state with geometrical parameters m and n, respectively

take STGNR(5,3) as example, and for the corresponding device, the spin-resolved I-V characteristics in P and AP configurations are manifested in Figs. 4 (a) and (b), respectively. Obviously, several important features can be visible: (1) In P configuration, the electron tunneling channels for both α- and β-spin states are almost blocked off completely, the negligible small currents ($< 5 \times 10^{-7}$ μA)in a region of interest can be observed. (2) In AP configuration, the unidirectional nature of the spin-polarized current shows up, namely, the α-spin channel is only opened under positive bias but suppressed fully under negative bias, while for the β-spin channel, it is just opposite. These mean that the STGNRs can act as a dual spin filter and a dual spin diode in AP configuration. (3) Making a comparison on currents between P and AP configurations, one can find that there is a much larger current (several μA) in AP configuration than that ($< 5 \times 10^{-7}$ μA)in P configuration, which implies that a switching magnetic field features a tremendous tuning effects on the spin transport and thus the giant magnetoresistance (MR) effect can be expected reasonably.

To understand the origin of distinctive transport behaviors, the relation of the transmission spectrum and electrode band structures under several typical biases, 0.0 and ±0.2 V, are displayed in Fig. 5(a) – (f), in which figures (a) – (c) and (d) – (f) correspond the P configuration and AP configuration, respectively. In each figure, the left, middle, and right panels show the band structure of the left electrode, the transmission spectrum of the device, and the band structure of the right electrode, respectively. To obtain a spin-dependent current, the band overlap is necessary, namely, the bands for the same spin state in two electrodes form an overlapping region in the bias window (BW) and make the electronic band-to-band tunneling available for carrying current. In P configuration, at zero bias, as shown in Fig. 5(b), the overlap of β- and α- spin bands in both electrodes above and below the Fermi level leads to two transmission peaks, respectively, but they do not contribute to the realistic electron transmission due to this transmission gap occurring around the Fermi level. When this device is negatively (positively) biased, the bands of the left and right electrodes are driven to move downward (upward) and upward (downward), respectively. Until - 0.2 (+0.2) V, as shown in Fig. 5(a) ((c)), no spin band overlap appears for the same spin state of two electrodes within the BW, resulting in the BW always lying in an transmission gap. And from then onwards, the transmission gap will increases monotonically with bias and the BW remains in between. Therefore, almost zero current arises in a device for P configuration regardless of the bias polarity and spin components. But for AP configurations, the situation is greatly changed. The applied switching magnetic field turns the role of α- and β-spin states in the right electrode to be exchanged each other, namely, minor and major spin components for α- and β-spin states, respectively. At zero bias, as shown in Fig. 5(e), no spin band overlap can be detected, and thereby no transmission peak occurs. However, when a negative bias is applied, the β-spin band in two electrodes approaches gradually and final overlapping, for example, at -0.2 V, as shown in Fig. 5(d), both of them have already a large overlap in the BW and generate a broaden and high transmission peak, thus a large β-spin current can emerge, while α-spin band in two electrodes goes far away gradually with bias, leading to a negligible small α-spin current. Under positive bias, behaviors for α (β)-spin state are similar to those for β(α)-spin state under negative bias, for example, at 0.2 V, as shown in Fig. 5(f), only α-spin band overlap occurs in the BW and creates a broaden and high transmission peak, and thus only a large α-spin current under positive bias is

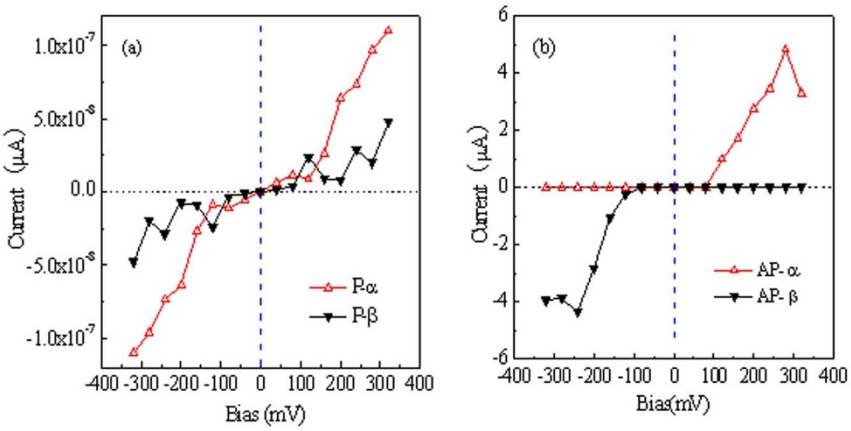

Figure 4 | The spin-resolved I-V characteristics in P (a) and AP (b) configurations for STGNR(5,3). In P configuration, the electron tunneling channels for both α- and β-spin states are almost blocked off completely, but in AP configuration, the bias-polarity-dependent spin-polarized current shows up.

derived. Remarkably, these obtained results are entirely consistent with those in Fig. 4.

To quantify the STD characteristics of STGNRs, we define the spin-independent rectification ratio as $RR_\sigma = \frac{|I_\sigma(\pm V)|}{|I_\sigma(\mp V)|}$ (σ = α, β), spin polarization as $SP_\sigma = \frac{I_\sigma}{I_{total}} \times 100\%$ (σ = α, β), and magnetoresistace as $MR = \frac{I_{Ap} - I_p}{I_p} \times 100\%$. The calculated results are shown in Fig. 6. As can be seen, an unexpectedly high rectification ratio, up to 10^{10}, can be reached in AP configuration, as shown in Fig. 6(a), which is a forward rectification for α-spin state and an inverse rectification for β-spin state. This rectification ratio is a much larger value as compared to that for a ZGNR diode (~10^5)[6] and macroscopic p-n junction diodes ($10^5 \sim 10^7$), this means that the STGNR can act as an excellent dual spin diode. And also, the perfect (100%) spin polarization is achieved under a slightly higher bias (≥0.1 V) in AP configuration regardless of a bias being positive or negative, as shown in Fig. 6(b), serving as a dual spin-filtering device, namely, by the selection of bias polarity, we can obtain an electron flow with different spin directions. More importantly, one can see that, by a switching magnetic field applied on STGNRs, a highly effective spin-valve device is likely to be realized, which displays a giant magnetoresistace (GMR) approaching 10^{10}%, which is three orders magnitude higher than that predicted based on the ZGNRs[5] and six orders magnitude higher than previously reported experimental values for the MgO tunnel junction[28–30].

Discussion

Spintronics and magnetic device properties of STGNRs are investigated theoretically. It is found that at a FM ground state the STGNRs always feature the typical properties of bipolar magnetic semiconductors. And their Curie temperature T_c is much higher as compared with that for ZGNRs. More importantly, the dual spin-filtering

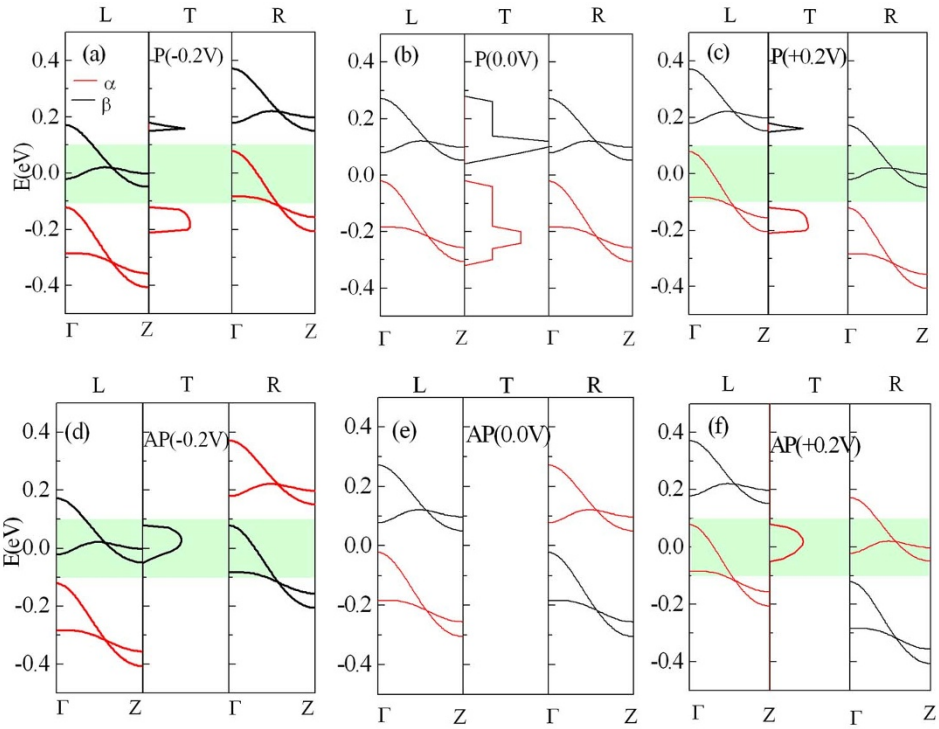

Figure 5 | The relation of the transmission spectrum and electrode band structures for STGNR(5,3) under several typical biases, 0.0 and ±0.2 V. (a) – (c) For P configuration. (d) – (f) For AP configuration. The region highlighted with green represents the bias window.

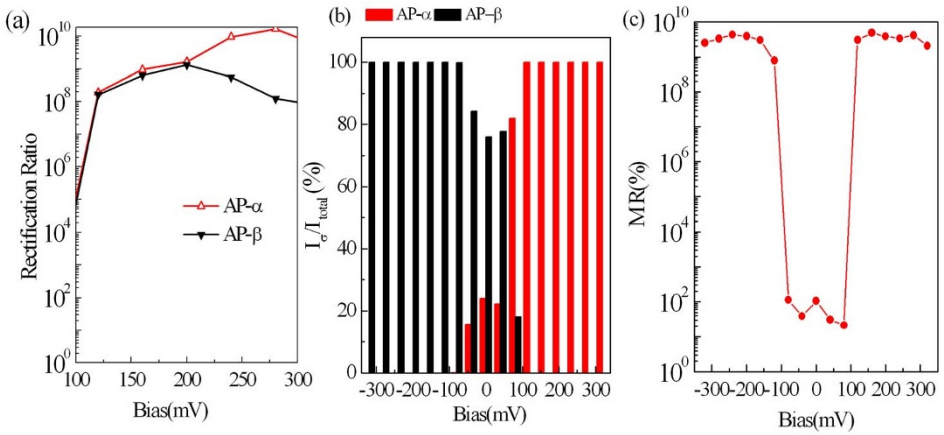

Figure 6 | The spin-independent rectification ratio (a) and spin polarization (b) in AP configuration as well as magnetoresistace (c) for STGNR(5,3). The high-performance dual spin diode effect with a rectification ratio about 10^{10} and the dual spin-filtering effect with the perfect (100%) spin polarization, as well as a giant magnetoresistace (GMR) value approaching 10^{10}%, can be achieved.

effect with the perfect (100%) spin polarization and high-performance dual spin diode effect with a rectification ratio about 10^{10} can be achieved, which is a much larger value as compared to that for a ZGNR diode ($\sim 10^5$) and macroscopic p-n junction diodes ($10^5 \sim 10^7$). Particularly, a highly effective spin-valve device is likely to be realized, which displays a giant magnetoresistace (GMR) approaching 10^{10}% that is three orders magnitude higher than the value predicted based on the ZGNRs and six orders magnitude higher than previously reported experimental values for the MgO tunnel junction. These distinctive features can be attributed to their unique band overlap pattern for two electrodes and particular sensitivity to a switching magnetic field. Our findings suggest that STGNRs have a promising performance for developing STDs.

As we know, there exist two types of hybridizations, sp^2- and sp^3-hybridizations, for edge carbon atoms of GNRs. Under a lower hydrogen-concentration, the usual edge structure is generally regarded to be the sp^2 hybridized mono-hydrogen termination. Therefore, mono-hydrogen terminated structures for GNRs are presented and investigated in most of literatures. In this present work, we also research on this type of termination for STGNRs. In fact, edge structure of GNRs is very diversified, such as dihydrogen termination[31], edge reconstruction[32], Z_{211} passivated edge[32], edge defects[32], and other chemical modifications, which might have an impact on magnetism. These complicated cases will be studied in our further works. Additionally, it might be difficult in achieving the required atomic precision for fabricating STGNRs in the current experiments, but theoretical modeling to understand the magnetic structure and magnetic transport properties of ideal STGNRs is very necessary.

Finally, we would like to point out that exchange -correlation functionals for DFT used in our work might underestimate the band gap of AGNRs compared with other algorithms, such as the GW method[33]. Therefore, a larger spin splitting energy gap E_g might occur if using other more exact methods for calculations. In our work, the spin polarization and spin diode effect as well as the spin-valve device effect are all closely related to the spin splitting energy gap, which would lead to need a higher threshold voltage to start spintronic device effects.

Methods

The geometric optimization as well as calculations of the electronic structure and transport are performed by using the spin-polarized DFT combined with the non-equilibrium Green's function(NEGF) method[34,35]. We employ Troullier-Martins norm-conserving pseudopotentials to represent the atom core and linear combinations of local atomic orbitals to expand the valence states of electrons. The spin-dependent generalized gradient approximation (SGGA) is used as the exchange–correlation functional is used as the exchange–correlation functional. The wave function is expanded by a single-zeta plus polarization (SZP) basis for H atoms, and double-zeta plus polarization (DZP) basis for other atoms. The k-point sampling is 1, 1, and 150 in the x, y, and z directions, respectively, where the z is the period direction of nanoribbon, and the cut off energy is set to 200 Ry. For all models studied, a 15Å vacuum slab is used to eliminate interaction between the models, and all calculation was performed after the geometries are optimized until all residual forces on each atom are smaller than 0.05 eV/Å. Once the convergence in self-consistency calculations is achieved, the spin-polarized current through a device is computed by the Landauer-like formula[36]. In our calculations, the average Fermi level, an average value of the chemical potential of the left and right electrodes, is set as zero.

1. Yazyev, O. V. Emergence of magnetism in graphene materials and nanostructures. *Rep. Prog. Phys.* **73**, 056501 (2010).
2. Pesin, D. & MacDonald, A. H. Spintronics and pseudospintronics in graphene and topological insulators. *Nat. Mater.* **11**, 409–416 (2012).
3. Dlubak, B. *et al.* Highly efficient spin transport in epitaxial graphene on SiC. *Nat. Phys.* **8**, 557–561 (2012).
4. Young-Woo Son, M. L. C. & Steven, G. Louie. Half-Metallic Graphene Nanoribbons. *Nature* **444**, 347–349 (2006).
5. Kim, W. Y. & Kim, K. S. Prediction of very large values of magnetoresistance in a graphene nanoribbon device. *Nat. Nanotechnol.* **3**, 408–412 (2008).
6. Zeng, J., Chen, K.-Q., He, J., Zhang, X.-J. & Sun, C. Q. Edge Hydrogenation-Induced Spin-Filtering and Rectifying Behaviors in the Graphene Nanoribbon Heterojunctions. *J. Phys. Chem.C* **115**, 25072–25076 (2011).
7. Zeng, M., Shen, L., Zhou, M., Zhang, C. & Feng, Y. Graphene-based bipolar spin diode and spin transistor: Rectification and amplification of spin-polarized current. *Phys. Rev. B* **83**, 115427 (2011).
8. Kan, E.-J., Li, Z., Yang, J. & Hou, J. Half-metallicity in edge-modified zigzag graphene nanoribbons. *J. Am. Chem. Soc.* **130**, 4224–4225 (2008).
9. Dutta, S., Manna, A. K. & Pati, S. K. Intrinsic half-metallicity in modified graphene nanoribbons. *Phys. Rev. Lett.* **102**, 096601 (2009).
10. Lin, X. & Ni, J. Half-metallicity in graphene nanoribbons with topological line defects. *Phys. Rev. B* **84**, 075461 (2011).
11. Li, X., Wu, X., Li, Z., Yang, J. & Hou, J. Bipolar magnetic semiconductors: a new class of spintronics materials. *Nanoscale* **4**, 5680–5685 (2012).
12. Pisani, L., Chan, J., Montanari, B. & Harrison, N. Electronic structure and magnetic properties of graphitic ribbons. *Phys. Rev. B* **75**, 064418 (2007).
13. Mermin, N. D. & Wagner, H. Absence of ferromagnetism or antiferromagnetism in one-or two-dimensional isotropic Heisenberg models. *Phys. Rev. Lett.* **17**, 1133–1136 (1966).
14. Areshkin, D. A. & White, C. T. Building blocks for integrated graphene circuits. *Nano Lett.* **7**, 3253–3259 (2007).
15. Li, Z., Qian, H., Wu, J., Gu, B.-L. & Duan, W. Role of Symmetry in the Transport Properties of Graphene Nanoribbons under Bias. *Phys. Rev. Lett.* **100**, 206802 (2008).
16. Kunstmann, J., Özdoğan, C., Quandt, A. & Fehske, H. Stability of edge states and edge magnetism in graphene nanoribbons. *Phys. Rev. B* **83**, 045414 (2011).
17. Yazyev, O. V. & Katsnelson, M. Magnetic correlations at graphene edges: basis for novel spintronics devices. *Phys. Rev. Lett.* **100**, 047209 (2008).
18. Sepioni, M. *et al.* Limits on intrinsic magnetism in graphene. *Phys. Rev. Lett.* **105**, 207205 (2010).
19. Saha, K. K., Nikolić, B. K., Meunier, V., Lu, W. & Bernholc, J. Quantum-interference- controlled three-terminal molecular transistors based on a single ring-shaped molecule connected to graphene nanoribbon electrodes. *Phys. Rev. Lett.* **105**, 236803 (2010).
20. Wang, Z. F., Jin, S. & Liu, F. Spatially separated spin carriers in spin-Semiconducting graphene nanoribbons. *Phys. Rev. Lett.* **111**, 096803 (2013).

21. Yu, D., Lupton, E. M., Gao, H. J., Zhang, C. & Liu, F. A unified geometric rule for designing nanomagnetism in graphene. *Nano Res.* **1**, 497–501 (2008).
22. Girao, E. C., Cruz-Silva, E. & Meunier, V. Electronic transport properties of assembled carbon nanoribbons. *ACS nano* **6**, 6483–6491 (2012).
23. Costa Girão, E., Liang, L., Cruz-Silva, E., Filho, A. G. S. & Meunier, V. Emergence of Atypical Properties in Assembled Graphene Nanoribbons. *Phys. Rev. Lett.* **107**, 135501 (2011).
24. Jia, X. *et al*. Controlled formation of sharp zigzag and armchair edges in graphitic nanoribbons. *Science* **323**, 1701–1705 (2009).
25. Zhang, J., Zhang, Z., Tang, G., Deng, X. & Fan, Z. Modulating magnetic ordering of the zigzag-edge trigonal graphene by functionalizations. *Org. Electron.* **15**, 1338–1346 (2014).
26. Narozhny, B., Aleiner, I. & Larkin, A. Magnetic fluctuations in two-dimensional metals close to the Stoner instability. *Phys. Rev. B* **62**, 14898 (2000).
27. Hynninen, T., Raebiger, H. & von Boehm, J. Structural and magnetic properties of (Ga,Mn)N from first principles. *Phys. Rev. B* **75**, 125208 (2007).
28. Parkin, S. S. *et al*. Giant tunnelling magnetoresistance at room temperature with MgO (100) tunnel barriers. *Nat. Mater.* **3**, 862–867 (2004).
29. Yuasa, S., Nagahama, T., Fukushima, A., Suzuki, Y. & Ando, K. Giant room-temperature magnetoresistance in single-crystal Fe/MgO/Fe magnetic tunnel junctions. *Nat. Mater.* **3**, 868–871 (2004).
30. Chopra, H. D., Sullivan, M. R., Armstrong, J. N. & Hua, S. Z. The quantum spin-valve in cobalt atomic point contacts. *Nat. Mater.* **4**, 832–837 (2005).
31. Sun, Y. Y. *et al*. Phase diagram of graphene nanoribbons and band-gap bifurcation of Dirac fermions under quantum confinement. *Phys. Rev. B* **85**, 195464 (2002).
32. Kunstmann, J., Ozdŏgan, C., Quandt, A. & Fehske, H. Stability of edge states and edge magnetism in graphene nanoribbons. *Phys. Rev. B* **83**, 045414 (2011).
33. Yang, L., Park, C.-H., Son, Y.-W., Cohen, M. L. & Louie, S. G. Quasiparticle energies and band gaps in graphene nanoribbons. *Phys. Rev. Lett.* **99**, 186801 (2007).
34. Brandbyge, M., Mozos, J.-L., Ordejón, P., Taylor, J. & Stokbro, K. Density-functional method for nonequilibrium electron transport. *Phys. Rev. B* **65**, 165401 (2002).
35. Pan, J., Zhang, Z., Deng, X., Qiu, M. & Guo, C. The transport properties of D-σ-A molecules: A strikingly opposite directional rectification. *Appl. Phys. Lett.* **98**, 013503 (2011).
36. Landauer, R. Electrical resistance of disordered one-dimensional lattices. *Philos. Mag.* **21**, 863–867 (1970).

Acknowledgments

This work was supported by the National Natural Science Foundation of China (Grant Nos. 61371065, 61101009, 61201080, and 51302022), the Construct Program of the Key Discipline in Hunan Province, Aid Program for Science and Technology Innovative Research Team in Higher Educational Instituions of Hunan Province, and the Scientific Research Innovation Fund for Postgraduate of Changsha University of Science and Technology.

Author contributions

Device design and theoretical analysis were performed by Z. Zg. Calculations for Electronic and magnetic structures, transmission spectra, and the I-V characteristics were performed mainly by D. W. and Secondarily by Z. Zu and B. L. All the authors discussed the results and wrote the manuscript.

Additional information

Competing financial interests: The authors declare no competing financial interests.

How to cite this article: Wang, D., Zhang, Z., Zhu, Z. & Liang, B. Magnetic structure and Magnetic transport Properties of Graphene Nanoribbons With Sawtooth Zigzag Edges. *Sci. Rep.* **4**, 7587; DOI:10.1038/srep07587 (2014).